Cadmium zinc telluride as a mid-infrared variable retarder

William FitzGerald, Saeid Taherion, F. Joseph Kumar, David Giles, and Dennis Hore

April 2018

This article was originally published at:
https://doi.org/10.1063/1.5020320

Journal of Applied Physics

Cadmium zinc telluride as a mid-infrared variable retarder

Cite as: J. Appl. Phys. **123**, 133103 (2018); https://doi.org/10.1063/1.5020320
Submitted: 22 December 2017 . Accepted: 18 March 2018 . Published Online: 05 April 2018

William FitzGerald, Saeid Taherion, F. Joseph Kumar, David Giles, and Dennis Hore

Cadmium zinc telluride as a mid-infrared variable retarder

William FitzGerald,[1] Saeid Taherion,[2] F. Joseph Kumar,[2] David Giles,[2] and Dennis Hore[1,a)]
[1]*Department of Chemistry, University of Victoria, Victoria, British Columbia V8W 3V6, Canada*
[2]*Redlen Technologies, 1763 Sean Heights Road, Saanichton, British Columbia V8M 1X6, Canada*

(Received 22 December 2017; accepted 18 March 2018; published online 5 April 2018)

The electro-optic behavior of cadmium zinc telluride is examined in the mid-infrared region between 3 and 11 μm, for applied DC field strengths of up to 10^6 V/m. The measurements performed here include full characterization of the polarization state of the transmitted light by means of the Stokes vector. We demonstrate the suitability of this material for DC variable retarder applications such as those achieved by quarter- or half-wave retardation. A comparison of two different metallic coatings for electrodes, gold and indium, reveals important differences in performance that are attributed to the homogeneity of the field through the bulk of the crystal. We illustrate that, in the case of both metals, the same electro-optic coefficients are measured, but regions of higher and lower retardation result in significant depolarization in the case of gold. Such depolarization may adversely affect the contrast ratio in a light valve, or increase the voltage necessary for the operation of an arbitrary polarization state generator. *Published by AIP Publishing.*
https://doi.org/10.1063/1.5020320

I. INTRODUCTION

Variable retarders are a class of materials that delay orthogonally polarized components of light with respect to one another by a tunable amount. Such retarders may be used for manipulating the polarization state of light that has application in a wide variety of optical instruments. For example, a quarter-wave retarder can be placed after a linear polarizer to create any polarization state by adjusting the relative azimuthal angle of the two components. A particular case is the creation of circularly polarized light when the amplitude along the fast- and slow-axes is equal. Being able to tune the retarder to achieve this quarter-wave condition across a range of wavelengths has application in chiroptical spectroscopy, where it has been recently demonstrated that DC retarders are better suited for sensitive polarization methods compared to AC devices.[1] A half-wave retarder can be used to rotate the azimuth of linearly polarized light by 90° in order to fully transmit or block a linear polarizer, creating a light valve which operates based on the state of the retarder. Achromatic optical retardation at a quarter- or half-wave level can be achieved in the infrared with rhomb designs of high-refractive index materials like ZnSe.[2–6] Depending on the type of variable retarder and the desired application, the retardation can be fixed at one value and then stepped, or it can be continuously changing with a set frequency. When fixed at one retardation, variable retarders can be useful for polarization state generation at different wavelengths, or as a light valve which switches on and off by alternating between half-wave retardation and no retardation. When the retardation is modulated continuously, the retarder can be useful in polarimetry and ellipsometry applications. Current devices available for variable retardation in various wavelength regions include mechanical devices such as Babinet-Soleil compensators,[7] electro-optic (EO) devices such as liquid crystals[8,9] and Pockels cells,[10] and photoelastic modulators.[11] Among these, Babinet-Soleil compensators and EO devices are capable of providing a fixed, yet tunable retardation.

Electro-optic materials provide an option for working in the mid-infrared, where materials for other types of retarders are more scarce than what is available in the visible and near-infrared. Two common EO phenomena include the optical Kerr and Pockels effects. In a Pockels cell, there is a linear relationship between the voltage applied to a material and the amount of birefringence. The original common materials for Pockels cells in the mid-infrared are ammonium dihydrogen phosphate, potassium dihydrogen phosphate or potassium dideuterium phosphate.[12,13] More recently, compounds of Group II and Group VI elements, known as II–VI compounds, have been used for this application, featuring wider band gaps and high stopping power for gamma detection. The material with the highest EO coefficient of all II–VI compounds is cadmium telluride (CdTe),[14] with r_{41} measured to be 6.8×10^{-12} m V^{-1} at both 3.39 and 10.6 μm,[15] though more recent measurements indicate a value of $5.5–5.9 \times 10^{-12}$ m V^{-1} at 10.6 μm.[16–18] Thus, cadmium telluride and other similar materials hold promise for electro-optic modulators and detectors in the infrared.[19–21]

Cadmium zinc telluride (CZT) is an alloy of cadmium telluride and zinc telluride. CZT materials are characterized by a formula $Cd_{1-x}Zn_xTe$, with x referring to the proportion of zinc substituted for cadmium with respect to CdTe, typically in the range 0–0.1[22] Like CdTe, CZT has a zinc-blende structure and belongs to the $\bar{4}3m$ space group. It is transparent from 1 to 20 μm, encompassing the entire mid-infrared region. CZT has been used as a photon-counting detector in the x-ray region, with higher resistivity and more suitable band gap than other available materials such as CdTe.[23,24] It is also known to display the Pockels effect, but while optical applications and properties of CdTe have been explored,[14]

a)Author to whom correspondence should be addressed: dkhore@uvic.ca

properties such as the electro-optic coefficient, the piezoelectric coefficient and the elasticity compliance tensors for CZT remain unexplored. The EO coefficient responsible for the Pockels effect in CZT, as with any zinc-blende crystal, is r_{41}, and the relationship of the voltage applied in the $[\bar{1}10]$ direction to the retardation with an optical axis in the [110] direction is given by

$$\delta = \frac{2\pi}{\lambda} n_0^3 r_{41} E \ell, \tag{1}$$

where ℓ is the distance the light travels through the crystal and E is the electric field strength the material experiences. The retardation δ refers to the amount of phase delay between orthogonal components of light with respect to a full wave. If we can assume that the electric field is uniformly distributed throughout the material, then $E = V/L$, where L is the distance between electrodes.

However, the semiconductor internal electric field profile is controlled by the properties of the metal-semiconductor interface, and the type of behaviour seen is dependent on the work functions of the metal, ϕ_M, and the semiconductor, ϕ_{CZT}. If $\phi_M < \phi_{CZT}$, then electrons flow from the metal into the semiconductor in order to balance the Fermi levels at the junction. This is known as an ohmic contact, and when a bias is applied across the crystal, the electric field is only dependent on less predictable surface characteristics including deep-level traps and dangling bonds but is ideally uniform through the material. On the other hand, if $\phi_M > \phi_{CZT}$, electrons flow from the semiconductor to the metal to balance the Fermi levels, and a potential barrier is developed which is a function of density of donors (or acceptors) at the surface and the difference in work functions ϕ_M–ϕ_{CZT}. A depletion region is created with a depth proportional to the square root of the potential barrier at each junction and the inverse of the density of donors (or acceptors). In electro-optic modulators of the type analyzed in this study, two such junctions exist on the sample on opposite faces, essentially back-to-back with one another. When a voltage is applied to the crystal, one junction becomes forward-biased and the other becomes reverse-biased, and in the reverse-biased junction, the depletion region becomes more severe as more electrons are drawn out of the semiconductor. Within the depletion region, the electric field drops approximately linearly, while it is constant outside of the depletion region. With an ohmic contact, no significant depletion region is expected. The crystal-metal junction is therefore an important characteristic of the performance of EO devices.[25]

Previously, we have reported on a new instrument for broadband Stokes polarimetry in the mid-infrared.[6] Using this instrument, we study the EO properties of CZT and evaluate its application as a variable retarder in the mid-infrared. Two CZT bars are studied, one with gold and one with indium electrodes. High-resistivity CZT has been reported as having a work function $\phi_{CZT} = 5.0\,\text{eV}$.[26] Gold has a work function $\phi_{Au} = 5.1\,\text{eV}$, and indium has the work function $\phi_{In} = 4.1\,\text{eV}$.[27] If the CZT work function falls between these two values, then one would anticipate that for indium, an ohmic contact should exist, leading to a relatively uniform electric field, while for gold, a depletion region and a gradient of electric field are expected.

II. EXPERIMENTAL

A. Cadmium zinc telluride EO crystals

The CZT samples characterized in this study were cut from a $Cd_{1-x}Zn_xTe$ single crystal boule, with x being nominally 0.1, grown at Redlen Technologies by their travelling heater method (THM). All six faces of the bars were sized by standard lapping methods and given a 0.3 μm polish as the final finish. On one crystal, two of the long sides opposite one another were metallized with gold, and gold wires are attached to one end of each metallized face. On the other crystal, the electrodes are indium, with gold wires attached. A specially designed enclosure shown in Fig. 1 relays the voltage from a cable to the crystal connections while allowing the sample to rest on a level surface, with no clamps or pressure applied. A second co-axial outlet enables measurement of the leakage current, which allows for measurement of the resistivity and can help avoid a short-circuit due to material breakdown. A 5 MΩ resistor in series between the crystal and the picoammeter limits short-circuit current to 1 mA. Two low-leakage 1N3595 diodes are installed in parallel to protect the picoammeter, and do not turn on during normal operation with the voltage below 200 mV. The circuit is housed in an aluminum enclosure, and a safe high voltage (SHV) connector shield connection is isolated from the enclosure, both of which reduce measurement noise. Figure 2 shows the leakage current of the two samples up to 10^6 V/m. Leakage current has been found to lead to material damage and short-circuit when it reaches 0.5 mA, but this

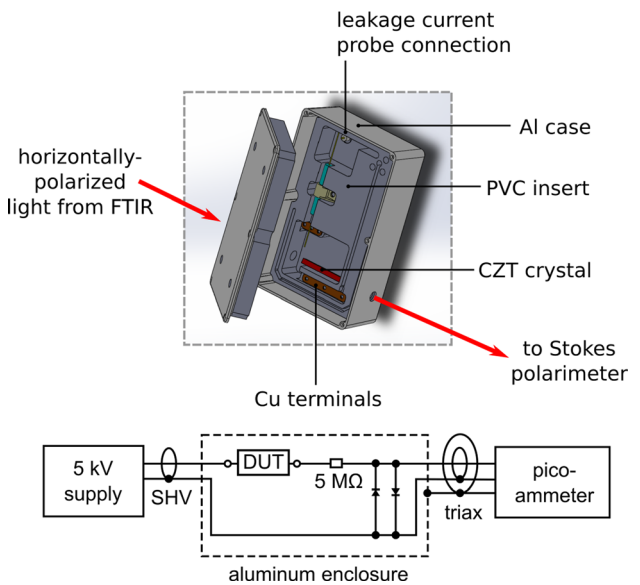

FIG. 1. Schematic of the sample holder. The CZT crystal (device under test or DUT) sits on a shelf in a single-piece poly(vinyl chloride) insert with no clamping. The enclosure provides a dark environment, with a small hole that enables the probe light to pass through the crystal long axis. The electronic components described by the schematic are contained within the upper portion of the enclosure and form a protection circuit for leakage current measurement.

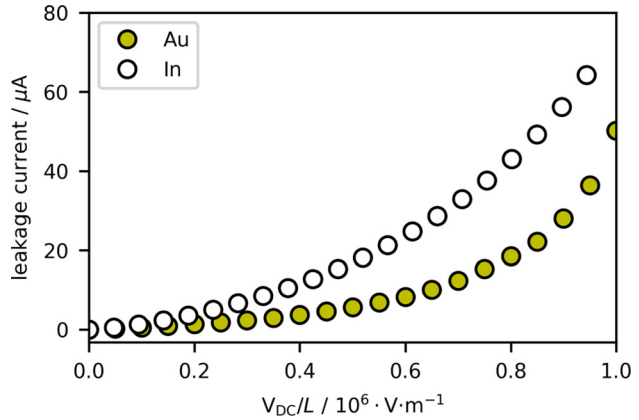

FIG. 2. Leakage current of two CZT samples with gold and indium electrodes, respectively.

threshold is not approached with the voltage applied. Comparing the two crystals in this experiment, the one with indium electrodes displays slightly higher leakage current than the one with gold electrodes. This follows the prediction of the uniformity of the electric field distribution as a result of the metal-semiconductor junction. In the gold electrode sample, a depletion region is expected to form due to the gold work function exceeding that of indium. This results in a region devoid of charge carriers, which presents a heightened barrier to current through the crystal. In the indium electrode sample, an ohmic contact with no depletion region is expected, and with a more uniform electric field through the crystal, less resistance to current is expected.

B. Broadband mid-infrared Stokes polarimetry

The polarization state of light may be fully described by the four-element Stokes vector **s**. In this description, s_0 represents the total intensity, s_1 the difference in intensities between components polarized horizontally and vertically, s_2 the difference between the orthogonal $\pm 45^\circ$ states, and s_3 the difference between right- (RCP) and left-handed circularly polarized (LCP) components

$$\mathbf{s} = \begin{bmatrix} s_0 \\ s_1 \\ s_2 \\ s_3 \end{bmatrix} = \begin{bmatrix} I_{\text{total}} \\ I_0 - I_{90} \\ I_{45} - I_{-45} \\ I_{\text{RCP}} - I_{\text{LCP}} \end{bmatrix} = \begin{bmatrix} E_x E_x^* + E_y E_y^* \\ E_x E_x^* - E_y E_y^* \\ E_x E_y^* + E_y E_x^* \\ i(E_x E_y^* - E_y E_x^*) \end{bmatrix}, \quad (2)$$

where E_x and E_y refer to the components of the electric field. Elements of the Stokes vector are related by

$$s_0^2 \leq s_1^2 + s_2^2 + s_3^2, \quad (3)$$

where the equality holds in the case of perfectly polarized light (no depolarization of the source). It is also convenient to define the degree of polarization, DOP, from the Stokes vector elements normalized to s_0

$$\text{DOP} = \sqrt{\left(\frac{s_1}{s_0}\right)^2 + \left(\frac{s_2}{s_0}\right)^2 + \left(\frac{s_3}{s_0}\right)^2}. \quad (4)$$

Fully polarized light has a degree of polarization (DOP) of unity. Equation (2) also illustrates that the Stokes vector is constructed from the x- and y-polarized components of the complex field, where $i = \sqrt{-1}$ and the asterisk denotes complex conjugation. This definition is useful as it readily enables modelling of the optical response and the optical properties of materials for comparison with experimental polarization data. If each of the four elements of **s** is measured independently, it is possible to describe the azimuth, the ellipticity, and the handedness of the polarization ellipse, in addition to the fraction of light that is depolarized. Many materials that display EO effects also depolarize the light as they modulate its polarization state. In some EO materials, the effect is quite significant. Often, the depolarization of light is attributed to small scattering bodies within the material. Such scattering is proportional to the inverse of the fourth power of the wavelength, and so is more pronounced at shorter wavelengths. Depolarization is also expected to occur if the entire beam of light does not encounter the same material properties within a material. When the Stokes vector of light resulting from transmission through a sample is a superposition of many different polarization states, the result is a degree of polarization less than one.

We have previously reported the design of a broadband, mid-infrared Stokes polarimeter which simultaneously measures the Stokes vector from 2.5 to 11 μm. Complete details of the instrument, calibration procedures, and data analysis to yield the Stokes vector are provided in Ref. 6. In brief, an FTIR in a step-scan mode is used as the source, followed by a wire-grid polarizer. After the light passes through the crystal, we direct the light through two photo-elastic modulators and a second wire-grid polarizer. Four lock-in amplifiers monitor four frequency components related to the photoelastic modulators and a chopper, producing four interferograms. Fourier transformation then yields spectra of the four Stokes vector elements. The incident light is polarized at 0° with respect to the polarimeter, and the crystal is mounted such that its optical axis develops at 45° as voltage is applied. This means that in measuring the resultant Stokes vector, s_2 should remain at zero so long as the only influence of the crystal on the polarization state results from the EO effect. From this, we can deduce the retardation of the crystal based on the ratio of s_3/s_1.

C. Polarized IR transmittance measurements

Another approach to measuring depolarization of light caused by transmission is to place the sample between two polarizers, with the front and back polarizers (analyzer) each azimuthally offset from the sample's optical axis by 45°. In one possible configuration, the polarizers are crossed with respect to one another. If the front polarizer is considered to be 0°, then the sample is at 45° and the analyzer at 90°. Transmittance can be determined by dividing the intensity of the light by the intensity measured with the analyzer removed. In the absence of any depolarization from the sample, no light would be transmitted through the analyzer at 0 V. As the voltage-dependent retardation increases, the transmittance increases until it reaches a maximum of unity

when the retardation reaches half-wave (π rad), where the light emerges polarized parallel to the analyzer. Beyond half-wave retardation, the transmittance then decreases until no light is transmitted at full-wave (2π rad) retardation. As the retardation encounters subsequent values of $n\pi$ rad, the transmittance oscillates between unity for odd n and 0 for even n. However, fully depolarized light (zero DOP) will always transmit exactly 50%. Thus, if a certain fraction D of the light becomes depolarized, the minimum possible transmittance through the analyzer is $D/2$. Similarly, the maximum transmittance is reduced to $1 - D/2$. If it is possible to achieve a retardation beyond the half-wave by varying either the wavelength or any other parameter, then this experiment can reveal the amount of depolarization from the sample. A complementary and confirmatory experimental scheme has the analyzer at 0°. In this scheme, the first extremum encountered is a minimum at half-wave retardation, with its divergence from zero revealing depolarization. The sum of the traces from these two experiments should always be unity, as the same light is encountering the analyzer in each case, and total light intensity is the sum of any two orthogonal components of the intensity. In the case of CZT, an FTIR spectrometer in a continuous scan mode is used as the source allows us to collect the transmittance spectrum across the mid-IR with a set voltage applied to the crystal. This method is applicable to measuring depolarization in CZT at a given wavelength provided that half-wave retardation is reached.

III. RESULTS AND DISCUSSION

A. Stokes polarimetry

Figure 3 shows the normalized Stokes vectors (each of the four Stokes vector elements divided by s_0) from 3 to 11 μm and up to 10^6 V/m. The left column shows the results for the Au-electrode sample, and the right column shows the results for the In-electrode sample. For both metals, the trends for the Stokes vector elements fit our expectations. At 0 V, we measure the incident state ($s_1 = 1$, $s_2 = s_3 = 0$), as the crystal is isotropic in the absence of an applied voltage. Because of the chosen experimental configuration (crystal optical axis at 45° with respect to the incident horizontal polarization), s_2 is expected to be zero at all voltages and wavelengths. As the retardation increases with voltage at any wavelength, s_1 drops from unity and oscillates, while s_3 increases from zero and then oscillates. Retardation changes are more dramatic at lower wavelengths, as expected. (A quarter-wave retardation at 6 μm corresponds to half-wave retardation at 3 μm.) Hence, it can be seen that each of s_1 and s_3 undergoes more oscillation towards 3 μm. On the shorter wavelength end of the spectrum, the maxima and minima of s_1 and s_3 fail to reach the values of 1 and –1, expected in the absence of any depolarization. The DOP across our 3–11 μm measurement range is shown in the bottom row of the figure. The Au-electrode sample has a significant reduction in DOP after crossing a threshold just below 0.2×10^6 V/m. The depolarization is greater at shorter wavelengths but does not increase consistently with the applied voltage. The In-electrode sample maintains a DOP close to unity across all wavelengths and voltages. The values of s_1 and s_3 are then

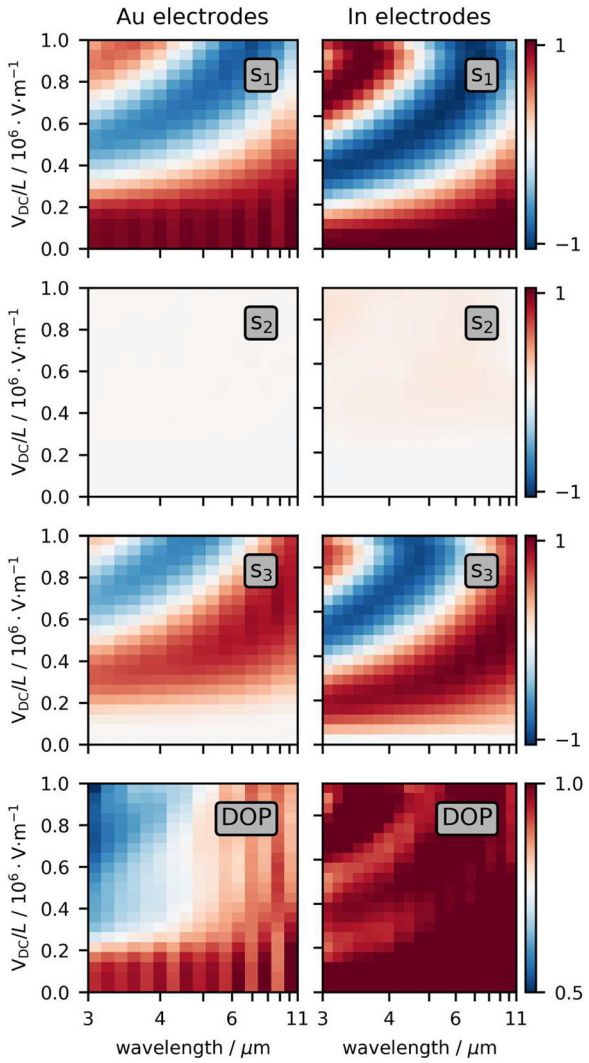

FIG. 3. The normalized Stokes vectors resulting from a linear polarizer with 0° linearly polarized light incident on a CZT sample with the optical axis oriented at 45°, measured at each wavelength across the instrument range, with the voltage applied to the crystal of up to 10^6 V/m. s_1, s_2, and s_3 are shown normalized to s_0, and these values are used to calculate the degree of polarization via Eq. (4).

used to calculate the retardation displayed in Fig. 4. Bold traces show the voltages required to achieve quarter- and half-wave retardation, of particular interest for applications in arbitrary polarization state generation and light valves. All of the trends match the expectation for a Pockels material, with the amount of retardation increasing with higher voltage and shorter wavelength. This analysis does not consider the depolarization; however, as the ratio s_3/s_1 is independent of DOP. What we obtain is the retardation of light considering only the polarized part which emerges from the sample. In the case of a light valve (half wave retardation), depolarization reduces contrast as it either diminishes the intensity of the transmitted "on" state or increases the level of the blocked "off" state. Nevertheless, the actual retardation of any such device is indicated in Fig. 4.

B. Polarized transmittance

In order to further study the observed depolarization, we used the more common experimental configuration

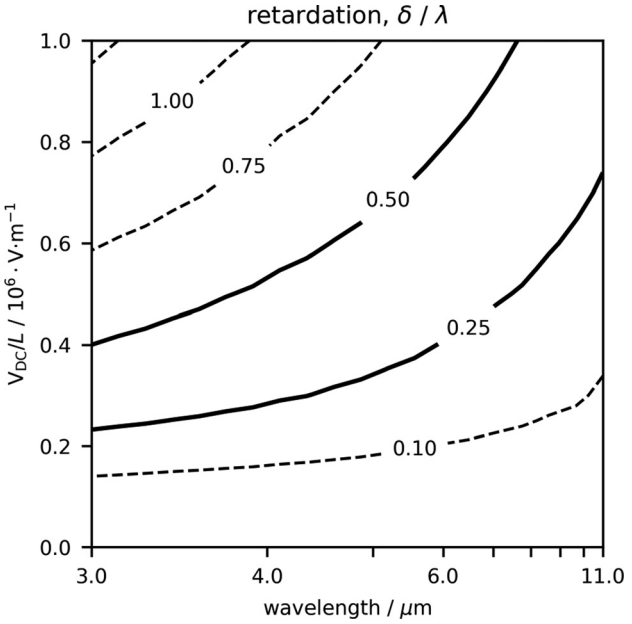

FIG. 4. Contours of the optical retardation of IR light by the CZT crystal with gold electrodes. The contours represent retardation with respect to the wavelength, so the 0.25 contour shows where quarter-wave retardation can be achieved at any wavelength in our measurement range.

consisting of the CZT sample between two polarizers. With the initial polarizer at the same orientation of 0° as in the Stokes polarimetry measurements, and the CZT sample with its optical axis 45° relative to this, the analyzer was oriented either parallel (0°) or crossed (90°) to the initial polarizer, and the transmittance was measured with the FTIR source working in a continuous scanning mode as a function of voltage from 0 to 1×10^6 V/m in steps of 250 V. The 0°–45°–0° spectrum obtained at 0 V was used as the reference spectrum, where light intensity is only affected by reflection loss. In a sample with no depolarization, the 0°–45°–90° configuration would be expected to show a transmittance of unity when a half-wave retardation is achieved, and a transmittance of zero when a full-wave retardation is achieved. The parallel polarizer configuration would be expected to show a transmittance of 0 when a half-wave retardation is achieved, and a transmittance of unity when a full-wave retardation is achieved.

The data for the gold sample are shown in Figs. 5(a) and 5(b). We can see that while the data display transmittance maxima and minima as higher voltage is applied, the maxima never reach unity and the minima are always above zero. Based on our Stokes polarimetry data, this can be attributed to depolarization. The amount of deviation from 1 and 0 is directly related to the amount of light that is being depolarized, and the same theories apply to full-wave and one-and-a-half wave retardation as seen at shorter wavelengths with higher applied voltage. As the voltage is increased, the wavelength at which maxima and minima are observed increases. At higher voltages, we see that they occur closer to their expected values at longer wavelengths. This is in keeping with the data in Fig. 3, as the DOP is higher at longer wavelengths at all voltages. The results obtained for the In electrode samples are shown in Figs. 5(c) and 5(d). It is apparent that the deviation between the maxima and unity, and between the minima and zero, is much less than in the case of the Au electrodes. Given the lower work function of the metal and the smaller or non-existent Schottky barrier with indium electrodes, this is expected. As there is still slight depolarization shown, we cannot say, for certain whether an ohmic contact is formed, or if the Schottky barrier is small.

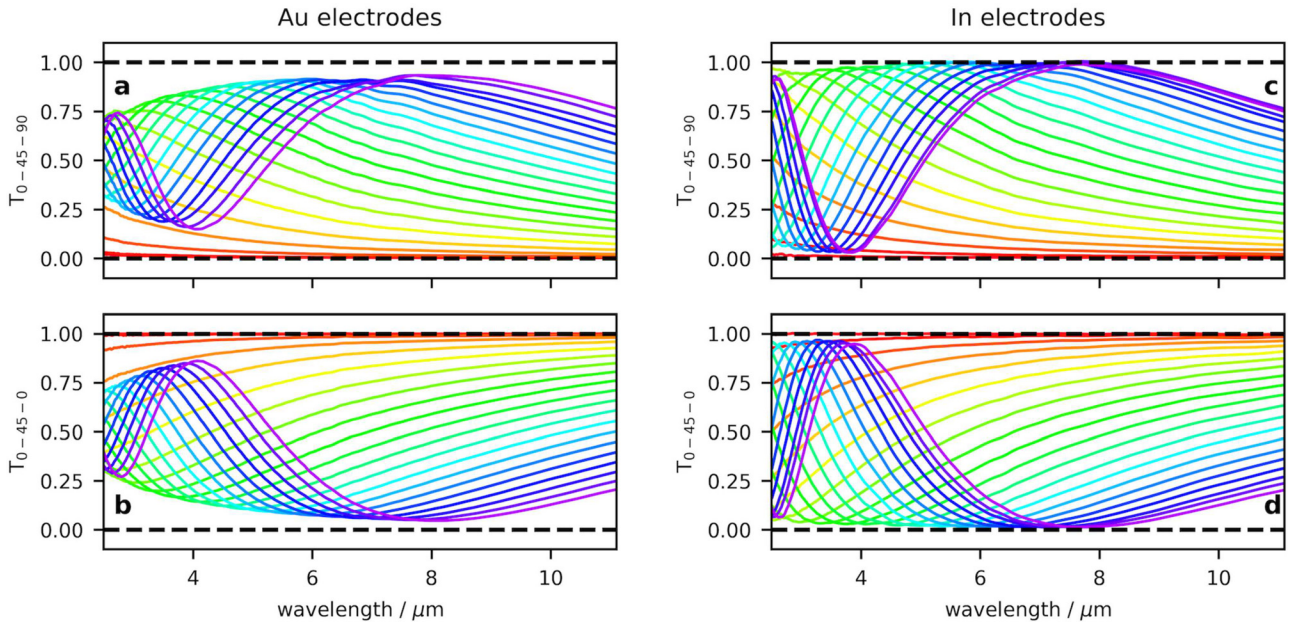

FIG. 5. For both CZT samples, the transmittance spectrum of light through 0°–45°–90° and 0°–45°–0° configurations of a polarizer–crystal–polarizer system, in a range of applied voltages (0 V/m in red progressing to 1×10^6 V/m for the Au-electrode sample, or to 0.95×10^6 V/m for the In-electrode sample, in violet). Data are normalized to the spectrum through parallel polarizers with no applied voltage to the crystal. The CZT optical axis is at 45° relative to the front polarizer. The gold electrode sample is shown in (a) and (b), with the indium electrode sample in (c) and (d).

C. Electric field distribution mapping

We suspect that the depletion region caused by the larger Schottky barrier in the Au-electrode sample can cause the electric field to be non-uniform through the crystal from one electrode to the other. If r_{41} is assumed to be constant within a single crystal sample with parallel incident and exit faces, Eq. (1) shows that retardation is proportional to the electric field strength. We can then attribute variation in retardation to variation in the electric field. The transmission through a crossed-polarizer system was mapped around the clear aperture in horizontal and vertical steps of 1 mm to cover an area of $40 \times 40\,\text{mm}^2$. A field of 0.2×10^6 V/m was applied to the crystal, low enough such that all wavelengths are below half-wave retardation. This ensures that increasing retardation will result in increased transmittance. The reference image was acquired with parallel polarizers at 0 V. The transmission values are divided by the reference values in order to eliminate any effects of beam clipping along the edges of the crystal and obtain the transmittance images in Fig. 6. Data obtained for the Au electrode crystal in Figs. 6(a) and 6(b) show the retardation decrease between the electrodes from one face of the crystal to the opposite face. When the direction of the applied voltage is flipped, this gradient in the electric field is reversed. This behaviour is consistent with an expected depletion region created within this sample from one electrode due to the Schottky barrier at the CZT-gold interface.

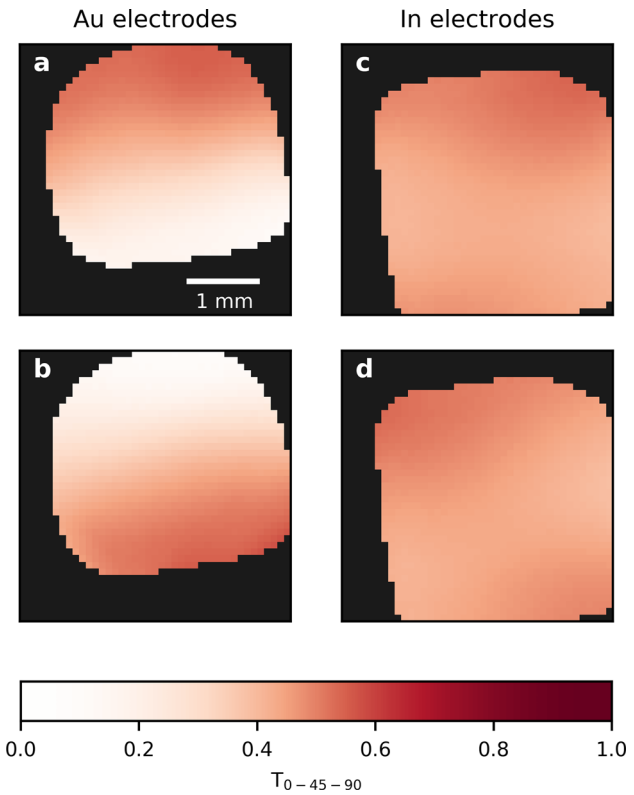

FIG. 6. The electric field of each crystal at 0.2×10^6 V/m applied voltage is imaged qualitatively in a 4 mm × 4 mm array. The electric field is taken as the amount of light transmitted through a 0°–45°–90° configuration, normalized to the amount of light obtained through a 0°–45°–0° configuration at 0 V. The aperture through which the crystal is viewed is restricted using a tape to ensure that no light reaches the detector after bypassing the crystal, and thus this aperture is smaller than the crystal itself. The gold sample is shown in (a) with the voltage applied from the top electrode and (b) with the voltage applied from the bottom electrode. The indium sample is shown in (c) with the voltage applied from the top electrode and (d) with the voltage applied from the bottom electrode.

We can use the depletion depth observed in the gold-electrode sample in Figs. 6(a) and 6(b) to confirm the n-type nature of CZT for our EO bars. We estimate the dielectric constant $\kappa_{CZT} = 10.9$, and the band gap $E_g = 1.57$ eV. The effective densities of states in the conduction (N_c) and valence (N_v) bands are calculated using the effective mass of an electron in CZT, m_e^{eff}, which is taken to be 0.15 times the mass of an electron, and the effective mass of a hole in CZT, m_p^{eff}, taken to be 0.73 times the mass of an electron. At 300 K

$$N_c = 2\left(\frac{2\pi m_e^{\text{eff}} k_B T}{h^2}\right)^{\frac{3}{2}} = 1.46 \times 10^{-18}\,\text{cm}^{-3}, \tag{5}$$

$$N_v = 2\left(\frac{2\pi m_p^{\text{eff}} k_B T}{h^2}\right)^{\frac{3}{2}} = 1.57 \times 10^{-19}\,\text{cm}^{-3}. \tag{6}$$

These values can then be used to calculate the intrinsic carrier concentration, n_i

$$n_i = \sqrt{N_c N_v}\exp\left(-\frac{E_g}{2k_B T}\right). \tag{7}$$

For an n-type semiconductor, the difference between the energy of the conduction band (E_c) and the Fermi level (E_f) is less than half of the band gap, and this value can be calculated using the donor density N_d from

$$E_c - E_f = \frac{E_g}{2} - k_B T \ln\left(\frac{N_d}{n_i}\right), \tag{8}$$

where donor density can be elucidated from

$$w = \sqrt{\frac{2\epsilon_0 \kappa_{CZT} V_a}{q N_d}}, \tag{9}$$

with ϵ_0 being the vacuum permittivity. We operate under the assumption that $V_a \gg V_b$, where V_b is the potential barrier and V_a is the applied voltage. The observed depletion depth w can thus be used to calculate a value for E_c–E_f. At 1 kV applied voltage, we observe a depletion depth within the gold-electrode sample of at least 3.0 mm, based on where the gradient is in observed retardation, and thus the electric field, tapers off. Using this value for w, E_c–E_f is calculated to be 0.45 eV, which confirms that CZT is an n-type semiconductor.

In the In electrode sample, shown in Figs. 6(c) and 6(d), the retardation is more consistent from one electrode to the other. There is no clear gradient, and though there are regions of higher retardation and lower retardation throughout the crystal, they do not appear to follow a steady monotonic increase or decrease from one electrode to the other. This indicates that no Schottky barrier is present, and the depolarization seen in the previous experiments is the result of other characteristics of the material such as deep-level traps, surface conditions, or dangling bonds. This informs us

that the work function of this CZT sample must be somewhere between the work functions of the two metals.

IV. MODELING

As the polarimetry, transmission, and imaging data all suggest a non-uniform electric field, a model can be created to account for the interaction of polarized light with the CZT crystals. This provides a route towards the full characterization of EO properties in the presence of depolarizing phenomena. As we are approximating the electric field as a linear gradient from the top to the bottom electrode, a distribution of retardation is modelled along this direction. If the beam was of uniform intensity with a circular cross-section, then we could model the distribution based on a circular geometry. However, due to the Gaussian nature of the beam, a normal distribution of retardations was considered

$$f(\delta) = \frac{1}{\sqrt{2\pi\sigma^2}} \exp\left[-\frac{(\delta - \bar{\delta})^2}{2\sigma^2}\right]. \tag{10}$$

with $\bar{\delta}$ being the mean retardation and σ the half-width of the distribution. The CZT material is taken to be a waveplate with its optical axis at 45°. The above distribution is then used to generate the Mueller matrix of the crystal

$$\mathbf{M}(\delta, 0^\circ) = \int_{-\infty}^{\infty} \begin{bmatrix} 1 & 0 & 0 & 0 \\ 0 & \cos\delta & 0 & \sin\delta \\ 0 & 0 & 1 & 0 \\ 0 & -\sin\delta & 0 & \cos\delta \end{bmatrix} f(\delta)\, \mathrm{d}\delta. \tag{11}$$

We numerically evaluate potential values for $\bar{\delta}$ and σ using this model Mueller matrix. In both Stokes vector and polarized transmission measurements, the initial Stokes vector represents horizontally polarized light as $\mathbf{s}_{\text{in}} = [1 \quad 1 \quad 0 \quad 0]^T$. In the case of the Stokes polarimetry data, we simulate the Stokes elements according to

$$\mathbf{s}_{\text{out}} = \mathbf{M}(\delta, 45^\circ) \cdot \mathbf{s}_{\text{in}}. \tag{12}$$

We can predict the intensity of light transmitted through the crossed-polarizer setup in a similar manner. The signal intensity is measured after encountering a linear polarizer at 90° after the sample

$$\mathbf{P}(90^\circ) = \frac{1}{2} \begin{bmatrix} 1 & -1 & 0 & 0 \\ -1 & 1 & 0 & 0 \\ 0 & 0 & 0 & 0 \\ 0 & 0 & 0 & 0 \end{bmatrix}, \tag{13}$$

and the transmittance can thus be calculated as the first element of the Stokes vector

$$\mathbf{s}_{\text{out}} = \mathbf{P}(90^\circ) \cdot \mathbf{M}(\delta, 45^\circ) \cdot \mathbf{s}_{\text{in}},$$

where

$$\mathbf{M}(\delta, 45^\circ) = \mathbf{R}(-45^\circ) \cdot \mathbf{M}(\delta, 0^\circ) \cdot \mathbf{R}(45^\circ),$$

with $\mathbf{R}$ being the standard Mueller rotation operator.[28] In Fig. 7, both of these fits are shown along with experimental data for the Au-electrode sample with 10^6 V/m applied voltage. The distribution of retardations used to generate the model is shown in Fig. 7(a). The retardation is shown in units of μm, as it allows a single quantity to represent the

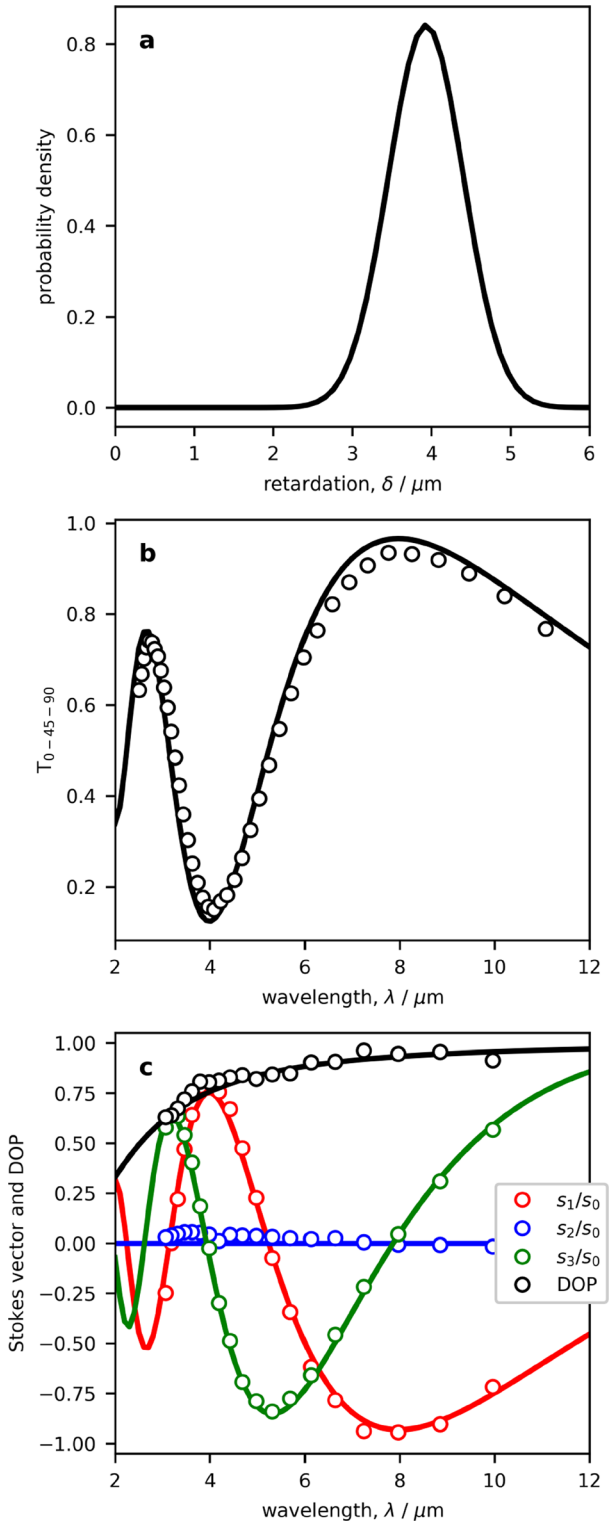

FIG. 7. Results of fitting the 1×10^6 V/m experimental data with Au electrodes to a model where depolarization results from a distribution of retardations. (a) The distribution of retardations probed by the IR light, (b) application of this model (solid line) to account for the transmittance in the 0°–45°–90° configuration with experimental data shown with points. (c) Application of the model (lines) to account for the measured Stokes vector elements (points) from 0°–45° configuration.

retardation at all wavelengths. For instance, the half-wave retardation at 4 μm would be quarter-wave retardation at 8 μm, and is reported simply as 2 μm retardation. In Fig. 7(b), the crossed-polarizer data are shown as black dots. In Fig. 7(c), the Stokes vectors are shown along with the DOP. The assumption that retardation scales with wavelength is valid provided that the properties of the material do not change significantly across our wavelength range, which is expected for this material. For the Stokes vector elements, and for the crossed-polarizer data, a higher mean retardation results in more oscillations. For instance, in the s_3 data in Fig. 7(c), the minimum near 5.5 μm will be shifted to lower wavelengths if the mean retardation is increased. The width of the model distribution affects the value of the maxima and minima. The most sensitive aspect of the data is the DOP. The width of the distribution of retardations directly relates to the extent to which the DOP decreases towards shorter wavelengths. Fitting the data to $\bar{\delta}$ and σ results in solid lines shown in Figs. 7(b) and 7(c), and is observed to well describe the data from both experiments. This fitting is then performed for each data set obtained at every applied voltage in the range. The same fitting was performed for the In-electrode crystal. The values of the mean retardation $\bar{\delta}$ [Fig. 8(a)] and the width of the distribution σ [Fig. 8(b)] divided by the length of the crystal, ℓ, can be compared between the two electrode metals. This is a dimensionless quantity when the retardation is expressed in distance units. The voltage applied is divided by the distance between electrodes on each crystal, L. This renders the slope in Fig. 8(a) to equal r_{41} multiplied by n_0^3. One observes that the slope in the mean retardations in the linear portions of the plot is very similar between the two crystals. This shows that the CZT electro-optic properties are essentially identical between the two samples. The difference in distribution widths, however, highlights the effect of the choice of metal in the electrode-CZT junction.

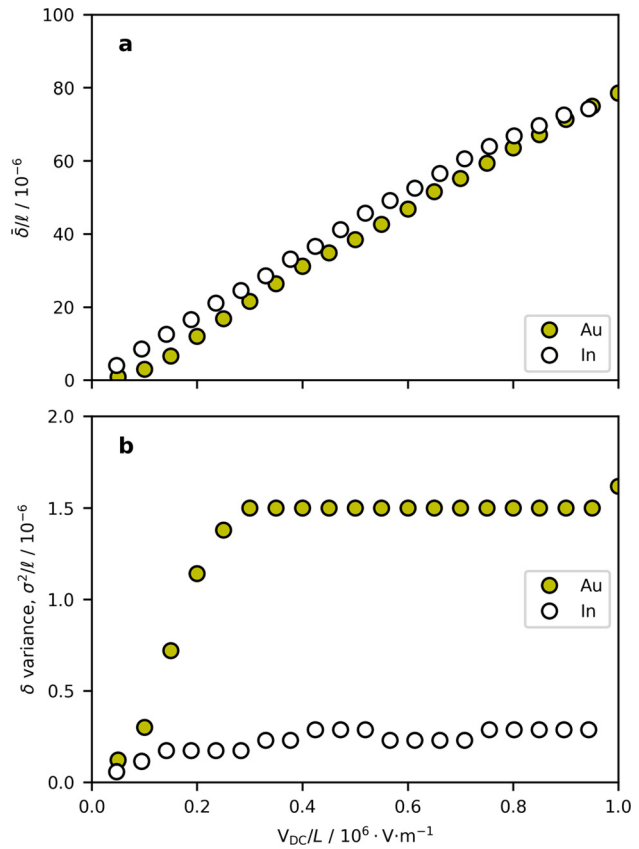

FIG. 8. The mean retardation and the width of the distribution whose best fit of both crossed-polarizer and Stokes polarimeter data is shown for each crystal.

With reference to Eq. (1), if the electric field is uniform, the r_{41} coefficient can be determined from

$$r_{41} = \frac{\delta L}{n_0^3 V \ell}, \tag{14}$$

with δ in distance units. The refractive index for CZT is not easy to measure in the mid-infrared. In theory, since there is no anti-reflection coating on these crystals, n_0 could be obtained from the normal incidence transmittance value. However, the presence of an oxide layer on the crystal entrance and exit faces, as well as the bulk defects in the material, complicate this determination. In order to estimate r_{41}, we can approximate the refractive index as being close to CdTe, which has a reported index of refraction of $n_0 = 2.70$ at 2.5 μm (Ref. 29) and $n_0 = 2.67$ at 10.6 μm.[30] The analysis to this point has shown that the electric field does not appear to be uniform for Au electrodes, even with a relatively low applied voltage. However, for the In electrode sample, the electric field variance (shown by the retardation distribution width in Fig. 8) is quite small. Using the slope of the linear fit, which is plotted in the top panel of Fig. 8, an approximate value for $n_0^3 \cdot r_{41}$ can be reported to be 8.54×10^{-11} m V^{-1}. As the model value is being used, this approach assumes that this value is not wavelength dependent. This would be consistent with the reported properties of CdTe,[15,31] and in addition, the modelling approach displayed in Fig. 7 uses a wavelength-independent value for r_{41} to generate the solid lines, and the fit to the experimental data at each voltage further supports this behaviour. The value determined for r_{41} using the estimated refractive index at 10.6 μm is 4.5×10^{-12} m V^{-1}. Such modelling is also useful as a predictive tool. We can use the determined mean and the width of the EO coefficient at various voltages to precisely predict the resultant polarization state and the degree of polarization when light is transmitted through an EO device which has been characterized in this manner.

V. CONCLUSION

We have used both Stokes polarimetry and polarized transmittance measurements to study the electro-optic properties of two CZT electro-optic modulators with different metals used as electrodes. Both crystals displayed similar EO coefficients, but differed in the degree of polarization of the transmitted light. In the case of In electrodes, there was virtually no depolarization, whereas a significant drop in the DOP was observed with Au electrodes. This difference was attributed to an inhomogeneity in the electric field distribution when using Au, resulting from a sizeable Schottky barrier at the metal-semiconductor junction. This barrier is not

present when low-work function indium is used for the electrodes instead. By creating a model for experimental results using a normal distribution of retardations, we have created a means to compare the ability of an EO device to function for optical retardation applications.

ACKNOWLEDGMENTS

We thank the Natural Sciences and Engineering Research Council of Canada (NSERC) for support of this science with Discovery, Engage, and RTI Grants. W.R.F. is grateful to NSERC, in collaboration with Redlen Technologies, for NSERC IPS-1 and IPS-2 graduate fellowships. Andrew Macdonald provided valuable assistance with the application of the DC field and designed the sample enclosure and its associated electronics. These parts were then machined by Chris Secord and Jeff Trafton.

[1]T. Narushima and H. Okamoto, Sci. Rep. **6**, 35731 (2016).
[2]D. H. Goldstein, *Polarized Light* (CRC Press, Boca Raton, FL, 2010).
[3]D. H. Goldstein, R. A. Chipman, and D. B. Chenault, Opt. Eng. **28**, 120 (1989).
[4]M. Kulish and S. Virko, Semicond. Phys. Quantum Electron. Optoelectron. **16**, 64 (2013).
[5]D. Mawet, C. Hanot, C. Lenaerts, P. Riaud, D. Defrère, D. Vandormael, J. Loicq, K. Fleury, J.-Y. Plesseria, J. Surdej, and S. Habraken, Opt. Express **15**, 12850 (2007).
[6]W. R. FitzGerald and D. K. Hore, J. Mod. Opt. **65**, 75 (2018).
[7]K. Oka and T. Kato, Opt. Lett. **24**, 1475 (1999).
[8]J. M. Bueno, J. Opt. A **2**, 216 (2000).
[9]J. S. Tyo, D. L. Goldstein, D. B. Chenault, and J. A. Shaw, Appl. Opt. **45**, 5453 (2006).
[10]T. W. King, G. L. Cote, R. J. McNichols, and M. J. Goetz, Opt. Eng. **33**, 2746 (1994).
[11]J. Cheng, L. Nafie, S. Allen, and A. Braunstein, Appl. Opt. **15**, 1960 (1976).
[12]J. H. Ott and T. Sliker, J. Opt. Soc. Am. **54**, 1442 (1964).
[13]W. R. Bosenberg, L. K. Cheng, and J. D. Bierlein, Appl. Phys. Lett. **65**, 2765 (1998).
[14]R. Bell, Rev. Phys. Appl. **12**, 391 (1977).
[15]J. Kiefer and A. Yariv, Appl. Phys. Lett. **15**, 26 (1969).
[16]G. L. Herrit and H. E. Reedy, MRS Proc. **152**, 169 (1989).
[17]D. Goldstein, "Polarization modulation in infrared electro-optic materials," Ph.D. thesis (University of Huntsville in Alabama, Huntsville, AL, 1990).
[18]D. Chenault, "Infrared spectropolarimetry," Ph.D. thesis (University of Huntsville in Alabama, Huntsville, AL, 1992).
[19]Q. Wu and X. Zhang, Appl. Phys. Lett. **71**, 1285 (1997).
[20]Q. Wu and X. Zhang, Appl. Phys. Lett. **68**, 2924 (1996).
[21]Q. Wu and X. Zhang, Appl. Phys. Lett. **68**, 1604 (1996).
[22]C. Szeles, Phys. Status Solidi B **241**, 783 (2004).
[23]Y. Eisen, A. Shor, and I. Mardor, Nucl. Instrum. Methods **428**, 158 (1999).
[24]Y. Eisen, A. Shor, and I. Mardor, IEEE Trans. Nucl. Sci. **51**, 1191 (2004).
[25]Z. Zhang and J. T. Yates, Jr., Chem. Rev. **112**, 5520 (2012).
[26]S. J. Bell, M. A. Baker, D. D. Duarte, A. Schneider, P. Seller, P. J. Sellin, M. C. Veale, and M. D. Wilson, J. Phys. D: Appl. Phys. **48**, 275304 (2015).
[27]S. Bell, M. Baker, H. Chen, P. Marthandam, V. Perumal, A. Schneider, P. Seller, P. Sellin, M. Veale, and M. Wilson, J. Phys. D: Appl. Phys. **46**, 455502 (2013).
[28]H. G. Tompkins and E. A. Irene, *Handbook of Ellipsometry* (William Andrew, Inc., Norwich, NY, 2005).
[29]D. Marple and H. Ehrenreich, Phys. Rev. Lett. **8**, 87 (1962).
[30]A. DeBell, E. Dereniak, J. Harvey, J. Nissley, J. Palmer, A. Selvarajan, and W. Wolfe, Appl. Opt. **18**, 3114 (1979).
[31]D. B. Chenault, R. A. Chipman, and S. Y. Lu, Appl. Opt. **33**, 7382 (1994).